ACS APPLIED MATERIALS & INTERFACES

www.acsami.org

Research Article

Enhancing Phototoxicity in Human Colorectal Tumor Cells Through Nanoarchitectonics for Synergistic Photothermal and Photodynamic Therapies

Alexandre Mendes de Almeida Junior,* André Satoshi Ferreira, Sabrina Aléssio Camacho, Lucas Gontijo Moreira, Karina Alves de Toledo, Osvaldo N. Oliveira, Jr., and Pedro Henrique Benites Aoki

Cite This: https://doi.org/10.1021/acsami.4c02247

Read Online

ACCESS | Metrics & More | Article Recommendations | Supporting Information

ABSTRACT: Phototherapies are promising for noninvasive treatment of aggressive tumors, especially when combining heat induction and oxidative processes. Herein, we show enhanced phototoxicity of gold shell-isolated nanorods conjugated with toluidine blue-O (AuSHINRs@TBO) against human colorectal tumor cells (Caco-2) with synergic effects of photothermal (PTT) and photodynamic therapies (PDT). Mitochondrial metabolic activity tests (MTT) performed on Caco-2 cell cultures indicated a photothermal effect from AuSHINRs owing to enhanced light absorption from the localized surface plasmon resonance (LSPR). The phototoxicity against Caco-2 cells was further increased with AuSHINRs@TBO where oxidative processes, such as hydroperoxidation, were also present, leading to a cell viability reduction from 85.5 to 39.0%. The molecular-level mechanisms responsible for these effects were investigated on bioinspired tumor membranes using Langmuir monolayers of Caco-2 lipid extract. Polarization-modulation infrared reflection−absorption spectroscopy (PM-IRRAS) revealed that the AuSHINRs@TBO incorporation is due to attractive electrostatic interactions with negatively charged groups of the Caco-2 lipid extract, resulting in the expansion of surface pressure isotherms. Upon irradiation, Caco-2 lipid extract monolayers containing AuSHINRs@TBO (1:1 v/v) exhibited ca. 1.0% increase in surface area. This is attributed to the generation of reactive oxygen species (ROS) and their interaction with Caco-2 lipid extract monolayers, leading to hydroperoxide formation. The oxidative effects are facilitated by AuSHINRs@TBO penetration into the polar groups of the extract, allowing oxidative reactions with carbon chain unsaturations. These mechanisms are consistent with findings from confocal fluorescence microscopy, where the Caco-2 plasma membrane was the primary site of the cell death induction process.

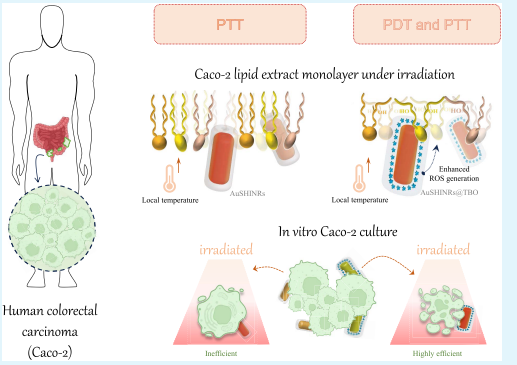

KEYWORDS: *gold shell-isolated nanorods (AuSHINRs), toluidine blue-O (TBO), human colorectal tumor cells (Caco-2), photodynamic therapy (PDT), photothermal therapy (PTT)*

INTRODUCTION

Gold nanorods (AuNRs), with their elongated axis design, are potent photothermal agents in photothermal therapy (PTT) due to their unique optical properties. This is primarily due to their adjustable localized surface plasmon resonance (LSPR) that enhances light absorption.[1−4] LSPR relates to the collective oscillation of conduction band electrons within the metal, resulting in localized heating around the nanorod.[5] This heat generation is crucial in PTT, particularly in treating tumors. When the temperature is elevated to the 40−47 °C, rapid cellular destruction occurs,[6,7] offering an approach for targeting hypoxic tumors that are often resistant to conventional treatments.[8−12] This thermal-induced damage is comprehensive, leading to irreversible effects like membrane plasmolysis, breakdown of vital proteins, and DNA alterations.[13−15] The difficulty in the extensive clinical use of AuNRs, though, lies in their instability in serum or blood environments.[16] This instability can lead to dissociation and aggregation, reducing their photothermal effectiveness in biological media depending on the ion concentration and pH.[17,18] This limitation can be circumvented by coating the AuNR with a silica shell, generating gold shell-isolated nanorods (AuSHINRs).[19] The silica coating stabilizes the nanorods while also preserving their biocompatibility and hydrophilicity, ensuring chemical robustness and transparency

Received: February 7, 2024
Revised: April 9, 2024
Accepted: April 10, 2024

to visible and near-infrared light, without altering the original plasmonic properties of the AuNRs significantly.[20,21]

Photothermal effects can be combined with photodamage of biological structures akin to photodynamic therapy (PDT).[22−24] The noninvasive nature of PDT provides a therapeutic benefit, without relying on molecular internalization,[25] through the interplay of three key elements: photosensitizers (PSs), oxygen present in cells, and a source of light for irradiation.[26−28] PSs, upon excitation by a specific light wavelength, transfer a portion of their absorbed energy to oxygen molecules, thus generating reactive oxygen species (ROS).[29] Two distinct pathways, known as type I and type II reactions, define these interactions.[30] Type I reactions involve the transfer of electrons from excited PSs to $^3O_2$, forming free radicals such as hydroxyls (OH^-), superoxides (O_2^{-}*) and hydrogen peroxide (H_2O_2).[31,32] Type II reactions transfer excitation energy, creating singlet oxygen ($^1O_2$), which is more cytotoxic and reactive toward cellular structures.[33,34] This makes the type II pathway preferred in PDT studies.[35] Additionally, the short lifetime of $^1O_2$ in biological systems (<0.04 μs) and their limited action radius (<0.02 μm) enable localized therapeutic action. In this context, toluidine blue-O (TBO) is distinguished as PS owing to its high quantum yield (Φ_Δ) of $^1O_2$ generation ($\Phi_\Delta{}^1O_2$ = 0.86), alongside its low excitation energy requirement (λ = 630 nm), minimal toxicity to mammalian cells and hydrophilic properties.[36,37]

In order to combine PTT and PDT, we produced a composite of AuSHINRs conjugated with TBO (AuSHINRs@TBO), aiming to enhance their effectiveness in cancer treatment. We employed human colorectal tumor cells (Caco-2) as therapeutic target, considering the high mortality rate and aggressive nature of colorectal cancer.[38] Additionally, there is a noticeable scarcity of research into the synergistic effects of photodynamic and photothermal therapies on such malignancies. Achieving a detailed understanding of the molecular effects induced by hyperthermia and photooxidation is crucial in this context. Hence, this study primarily focused on determining the molecular-level interactions and photoinduced effects of AuSHINRs@TBO on the plasma membrane, which is a critical target and barrier in therapeutic applications. Lipid extracts isolated from Caco-2 cell cultures were assembled in Langmuir films as a model system to mimic tumor membranes. The lipid composition of Caco-2 reflects typical characteristics of colorectal tumors, mainly composed of phosphatidylcholines, phosphatidylethanolamines, and sphingomyelins.[39] Variations may exist depending on the origin of the tumor, the microenvironment, and metabolic status.[40] Evidence of AuSHINRs@TBO adsorption was provided by surface pressure isotherms, while the molecular-level interactions were investigated with polarization-modulation infrared reflection−absorption spectroscopy (PM-IRRAS). Experiments with Caco-2 *in vitro* cell cultures demonstrated that AuSHINRs@TBO are highly efficient in reducing cell viability upon light irradiation. As we shall demonstrate, the TBO-conjugated nanorods enhanced the generation of ROS toward the convergence of photothermal effects and oxidative reactions, which is promising for a potent and targeted therapeutic impact against cancer cells.

MATERIALS AND METHODS

Preparation and Characterization of Gold Shell-Isolated Nanorods Conjugated with Toluidine Blue-O (AuSHINRs@TBO). Gold nanorods (AuNRs) were synthesized using a well-established method,[41] where colloidal seeds were made by mixing 10 mL of CTAB at 0.1 mol/L with 50 μL of $HAuCl_4$ at 0.05 mol/L in a beaker. This mixture was stirred at 28 °C until it turned yellow. Subsequently, the stirring was intensified, and 600 μL of $NaBH_4$ at 10 mmol/L was introduced, resulting in a change of the colloid color to yellow-brownish. The obtained seeds were kept untouched for a while prior to use. For the growth of the seeds, 20 mL of CTAB at 0.1 mol/L, 70 μL of $AgNO_3$ at 4 mmol/L, 200 μL of $HauCl_4$ at 0.05 mol/L, and 200 μL of ascorbic acid at 0.1 mol/L were sequentially added. 48 μL of the prepared seeds were introduced into this solution. The reaction was completed in about half hour, resulting in a dark blue colloid. The AuNRs colloid was left undisturbed for 24 h hidden from the light at room temperature. Gold shell-isolated nanorods (AuSHINRs) were obtained by alkalizing the AuNRs colloid with the addition of NaOH at 1 mol/L until the pH reached 10.5. The resulting colloid was then poured to a flask and vigorously stirred at 28 °C. Three 300 μL volumes of TEOS (20% v/v in methanol) were added every 30 min, with the colloid stirred for 24 h. In parallel, a silica-TBO precursor was prepared, following the methodology described by Grandi et al.[42] In brief, 1.69×10^{-5} mol of TBO (16.92 mL of 1×10^{-5} mol/L) was mixed with 1.69×10^{-5} mol of 3-(triethoxysilyl)propyl isocyanate (42 μL of 4 mol/L) in a flask under vigorous stirring for 24 h. AuSHINRs conjugated with TBO (AuSHINRs@TBO) were obtained by mixing 1.7 mL of the silica-TBO precursor with 10 mL of the AuSHINRs (3.6×10^{11} nanoparticles/mL) colloid, allowing the mixture to stir for 30 min. A final silica shell was placed with additions of 50 μL TEOS (20% v/v in methanol) at 30 min intervals, during vigorous stirring for 24 h.

The synthesized AuSHINRs@TBO underwent three cycles of centrifugation at 12000 rpm for 10 min each to eliminate excess of CTAB. At every cycle, the sedimented particles were resuspended in ultrapure water, while the supernatant was discarded. Table S1 lists the hydrodynamic diameters (nm) obtained from dynamic light scattering (DLS) for each rinsing step. Characterization of AuNRs, AuSHINRs, and AuSHINRs@TBO involved UV−Vis absorption spectroscopy (Agilent Cary 60), ζ potential (Malvern Panalytical, Zetasizer Nano S90), fluorescence (630 nm, Renishaw in-ViA), and transmission electron microscopy (120 kV FEI Tecnai). The photothermal efficiency of the AuSHINRs and AuSHINRs@TBO was evaluated by photoactivating the colloid at 630 nm with 20 mW/cm^2 LED source (BioLambda).

Caco-2 Cell Culture. Human colorectal carcinoma (Caco-2, ref 0059) cells were purchased from the Cell Bank of Rio de Janeiro (RJ, Brazil), cultured in RPMI medium (ref 23400021, Gibco) containing antibiotic-antimycotic (ref 15240−062, Thermo), supplemented with 10% v/v of fetal bovine serum (FBS; ref 0521-500, Cultilab, Campinas, SP, Brazil), and grown in T-75 cm^2 flasks (ref 3290, Corning Glass Works, Corning, NY). The cells were manipulated in a sterile environment, and the incubation conditions were kept at 37 °C and 5% of CO_2. The cellular cultivation involved media replacement with RPMI every 48 h and passaging once a week when cell confluency reached a minimum of 80%. Cells were rinsed with 5 mL of phosphate-buffered saline (PBS), detached from the T-flask using 1 mL trypsin, and then plated in a 96-well plate for 24 h to achieve a confluency of ≥80%. The remaining harvested cells were transferred to a new T-flask containing fresh media for ongoing cultivation. Cell viability was assessed through the mitochondrial metabolic activity (MTT) assay [3-(4,5-dimethylthiazol-2-yl)-2,5-diphenyltetrazolium bromide] (reference: M2003; Sigma-Aldrich). The Caco-2 cells seeded in 96-well plate underwent incubation with different proportions of AuSHINRs and AuSHINRs@TBO (ranging from 1:7, 1:8, 1:9, to 1:10 v/v in culture medium) for 1 h. Cells cultured in the absence of nanoparticles were designated as the 100% viable cellular control (CC), and the introduction of hydrogen peroxide was employed as the death control (DC). The Caco-2 culture was irradiated for 1 h using the LED system (BioLambda) connected to a digital controller, set at 640 nm and 20 mW/cm^2. Irradiated cells in RPMI (without AuSHINRs) were designated as the cellular light control (LC). The culture medium was then replaced by PBS and gently washed, followed by incubation (40−60 min) with 0.5 g/L of

https://doi.org/10.1021/acsami.4c02247
ACS Appl. Mater. Interfaces XXXX, XXX, XXX−XXX

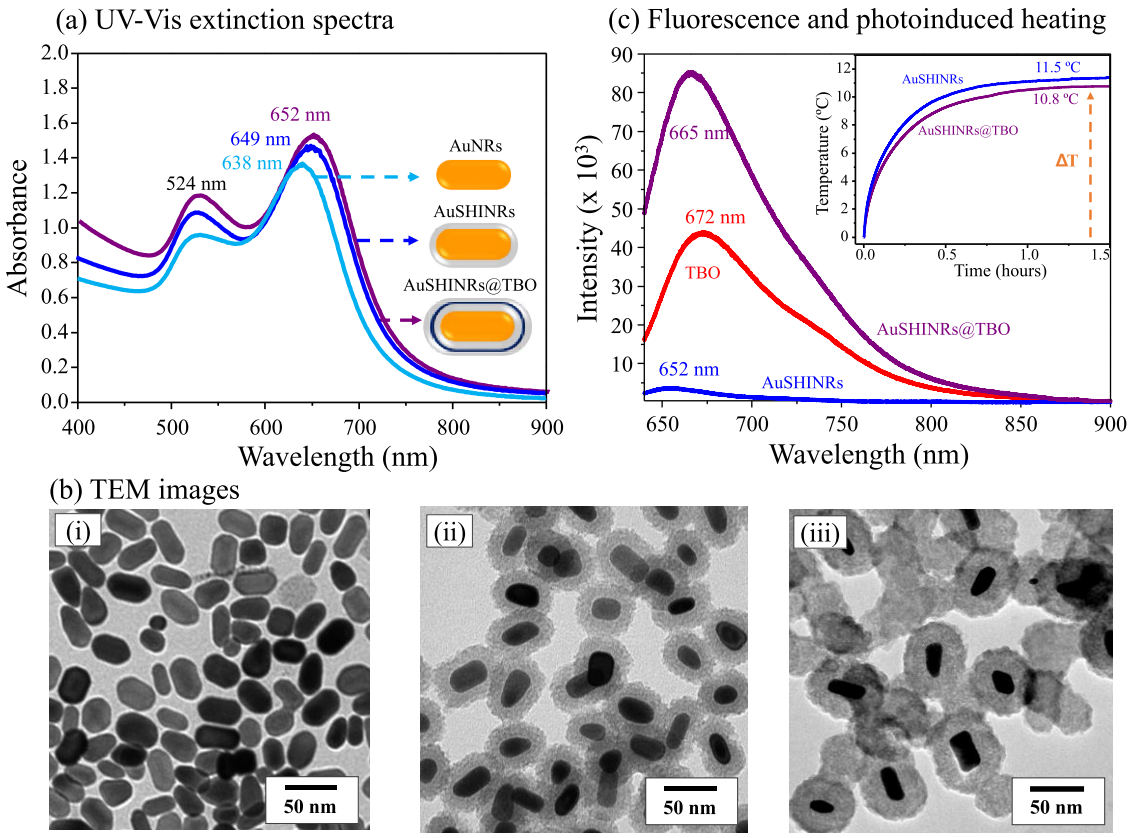

Figure 1. (a) UV−Vis spectra of AuNRs, AuSHINRs, and AuSHINRs@TBO, all diluted in ultrapure water (1:1 v/v). (b) TEM images captured for (i) AuNRs, (ii) AuSHINRs, and (iii) AuSHINRs@TBO. (c) Fluorescence spectrum of AuSHINRs, TBO (10^{-3} mol/L) solution, and AuSHINRs@TBO suspension, respectively. The Inset shows the photoinduced heating of AuSHINRs and AuSHINRs@TBO at a 630 nm LED source (20 mW/cm^2).

MTT. Dimethyl sulfoxide (DMSO) at 50×10^{-6} L was added to the wells to solubilize the formazan crystals, and absorbance was performed using a Multiskan FC microplate photometer at 560 nm.

Caco-2 Lipid Extraction. The cells were detached and collected using trypsin (4 min at 37 °C), and then separated into Falcon tubes for centrifugation at 1500 rpm for 5 min. After the supernatant was removed, 1×10^{-3} L of ultrapure water was added and submitted to vortex for 10 min. Subsequently, 4×10^{-3} L of chloroform were added, and the mixture was subjected to an additional 10 min of vortex stirring and 30 min of sonication. The resulting solution formed two distinct phases, one consisting of water-soluble cellular components and the other containing chloroform-soluble fragments. The earlier was discarded, leaving only the chloroform phase enriched with Caco-2 lipid structures. The final solution was transferred to a glass vial and stored in an −20 °C freezer.

Langmuir Monolayers and Characterization of Caco-2 Lipid Extract. Langmuir monolayers of Caco-2 lipid extract were assembled using a KSV-NIMA (KN1002, Biolin Scientific) trough by spreading the lipid extract solution on a subphase of a phosphate-buffered saline (PBS) solution (pH 7.4). The initial concentration of the AuSHINRs@TBO colloid was doubled, followed by cospreading with Caco-2 lipid extract in varying fractions of 10:1, 5:1, and 1:1 v/v (Caco-2: AuSHINRs@TBO). Prior to the beginning of each experiment, the solvent was left to evaporate for 10 min and the subphase temperature was kept at 21 °C using the ultrathermostatic bath (SolidShell SSDu−10 L). Surface pressure (π) versus area (A) isotherms were obtained through the Wilhelmy method, employing a platinum rod, during the symmetric closing of the barriers at 5 mm/min.[43] To ensure reproducibility within ±2 mN/m, at least 3 experiments were conducted for each π−A isotherm. Irradiation experiments were conducted at a surface pressure of 30 mN/m with a 630 nm (20 mW/cm^2) LED (BioLambda) installed 20 cm over the Langmuir films. PM-IRRAS measurements were carried out in a KSV PMI550 (KSV, Finland) trough, with spectra recorded for neat Caco-2 lipid extract and Caco-2: AuSHINRs@TBO (1:1 v/v) monolayers at 30 mN/m, both before and after irradiation. Spectra reproducibility was ensured to attribute band shifts to AuSHINRs@TBO adsorption and subsequent photooxidation rather than variability in the results. Brewster angle microscopy (BAM) images were captured by using an Accurion (Nanofilm EP4) microscope coupled to the Langmuir trough. This setup allowed real-time evaluation of extract domains on PBS, in the presence and absence of AuSHINRs@TBO (1:1 v/v of Caco-2 lipid extract).

RESULTS AND DISCUSSION

Gold Shell-Isolated Nanorods Conjugated with Toluidine Blue-O (AuSHINRs@TBO). Figures 1a,b display the UV−Vis extinction spectra and transmission electron microscopies (TEM) of AuNRs, AuSHINRs, and AuSHINRs@TBO, respectively. The initial extinction band at 524 nm refers to the transversal localized surface plasmon resonance (LSPR), while the band at 638 nm is assigned to the longitudinal LSPR.[41,44,45] The length (L) and width (W) of the nanorods were measured from the TEM images in Figure S1, yielding an aspect ratio (AR = L/W) close to 1.9. The latter is coherent with the longitudinal band absorption in red light (~630 to 660 nm),[41,44,45] within the targeted therapeutic window.[44,46] With silica coating, the longitudinal LSPR shifts from 638 to 649 nm owing to a change in the refractive index of AuSHINRs.[41,47−49] Conjugation with toluidine blue-O (TBO) did not induce a displacement in the extinction spectra. However, the final silica coating caused a slight shift in the longitudinal LSPR to 652 nm. The ζ potential in Table 1

https://doi.org/10.1021/acsami.4c02247
ACS Appl. Mater. Interfaces XXXX, XXX, XXX−XXX

Table 1. ζ Potential and Average Silica Shell Thickness of AuSHINRs and AuSHINRs@TBO

nanostructures	ζ potential (mV)	average silica thickness by TEM (nm)
AuSHINRs	+25 ± 1	SS = 15 ± 2
AuSHINRs@TBO	+29 ± 5	SS = 24 ± 1

increased from +25 mV ± 1 for AuSHINRs to +29 mV ± 5 for AuSHINRs@TBO owing to the conjugation with the cationic TBO. As evidenced in other studies, the second silica layer diminishes the impact of the charge, resulting in small differences between the two samples.[50−52]

Figure 1c shows the fluorescence spectra of TBO (10^{-5} mol/L), AuSHINRs, and AuSHINRs@TBO. While the exact concentration of TBO conjugated to the AuSHINRs is unknown, it is reasonable to presume that it must be below 10^{-6} mol/L, as this was the initial concentration employed for the conjugation process. Due to conjugation, the TBO emission shifts from 672 to 665 nm, and the fluorescence intensity of AuSHINRs@TBO increased notably. This surface enhancement[54,55] can be attributed to the enhanced electromagnetic environment near the metal surface, resulting in intensified fluorescence signals. The inclusion of a silica layer mitigates quenching by establishing a suitable distance between the dye and the metal.[54,56−58] Therefore, the surface-enhanced fluorescence (SEF) further supports the successful conjugation of TBO with AuSHINRs. The inset in Figure 1c depicts the heat conversion of AuSHINRs@TBO under irradiation, reaching a plateau in the temperature at approximately 11 °C. A comparison with the heat conversion capacity of AuSHINRs without TBO reveals a similar increase in temperature, confirming that the conjugation with TBO and the addition of an extra silica shell did not compromise the photothermal efficiency of the AuSHINRs.[53]

AuSHINRs@TBO Incorporation into Caco-2 Langmuir Monolayers. The π−A isotherms of Caco-2 lipid extract, AuSHINRs@TBO, and Caco-2: AuSHINRs@TBO mixtures (10:1, 5:1 and 1:1 v/v) on PBS are displayed in Figure 2a. AuSHINRs@TBO on PBS was surface active owing to the salting-out effect.[59] According to Table 2, increasing the volume of the colloid within Caco-2 mixed films causes a shift in the π−A isotherms toward larger molecular areas, indicating incorporation of AuSHINRs@TBO. Earlier investigations suggested that incorporation of AuSHINRs[53] and TBO[60] into bioinspired membranes is driven by attractive electrostatic interactions with negatively charged groups in the phospholipid polar heads. Nontumoral cell membranes are asymmetric, with phosphatidylcholines (PC) predominantly in the outer leaflet and phosphatidylserines (PS) primarily located in the inner leaflet.[61] In tumoral cells, this inherent asymmetry is disrupted, as PS is also in the outer leaflet of the cell membrane.[62−64] PS typically bear negative charges in their polar region, stemming from phosphate and carboxylic groups, potentially favoring attractive forces with AuSHINRs@TBO (ζ = +29 mV). Nevertheless, the presence of positively charged groups in the lipid extract may also play a role and hinder adsorption of nanorods onto membranes due to repulsive forces.[53]

Table 2. Relative Shifts in Area Per Lipid $[(A - A_0)/A_0] \times 100$ Induced by Incorporation of AuSHINRs@TBO[a]

extract/nanostructures ratio	relative shift $[(A - A_0)/A_0] \times 100$
Caco-2/AuSHINRs@TBO (10:1)	0.3% ± 1.6
Caco-2/AuSHINRs@TBO (5:1)	11.2% ± 1.6
Caco-2/AuSHINRs@TBO (1:1)	57.1% ± 2.3

[a] A_0 is the extrapolated area at 30 mN/m on PBS, and A is the corresponding extrapolated area in the presence of AuSHINRs@TBO.

Figure 2b shows BAM images for neat Caco-2 lipid extract monolayers and those containing AuSHINRs@TBO (1:1 v/v Caco-2 lipid extract). Our focus was on the highest proportion of conjugated nanostructures, chosen for its noteworthy isotherm displacements. In Caco-2 monolayers, no distinction

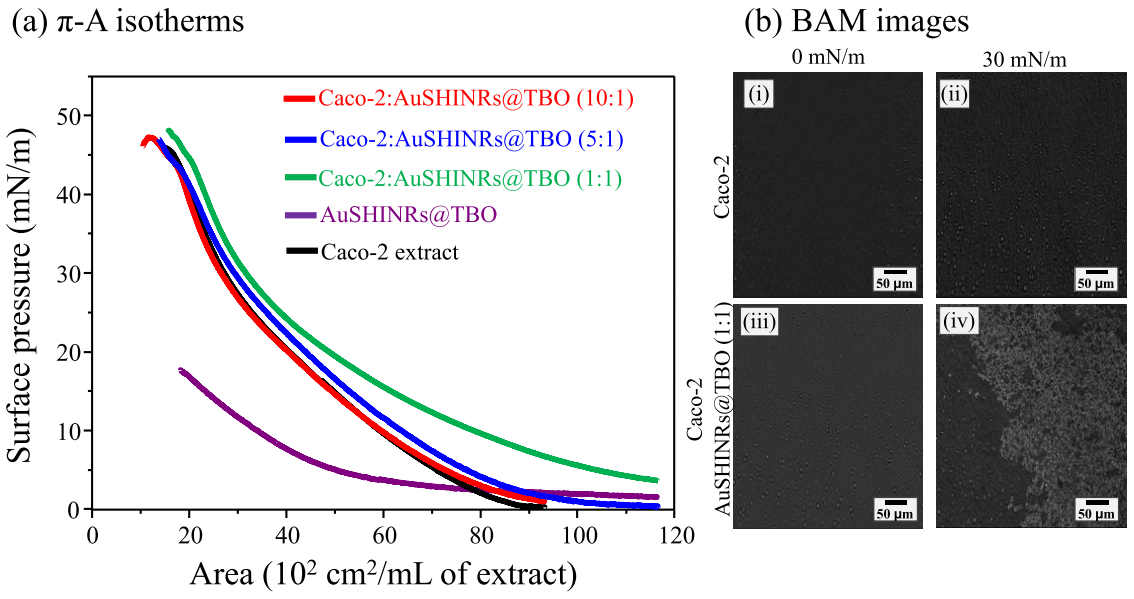

Figure 2. (a) π−A Isotherms of Caco-2 lipid extract, AuSHINRs@TBO colloid, and Caco-2: AuSHINRs@TBO mixtures (10:1, 5:1 and 1:1 v/v) on PBS (b) Brewster angle microscopy (BAM) images registered at 0 and 30 mN/m for (i), (ii) Caco-2 lipid extract, (iii), and (iv) Caco-2: AuSHINRs@TBO mixtures (1:1 v/v).

https://doi.org/10.1021/acsami.4c02247
ACS Appl. Mater. Interfaces XXXX, XXX, XXX−XXX

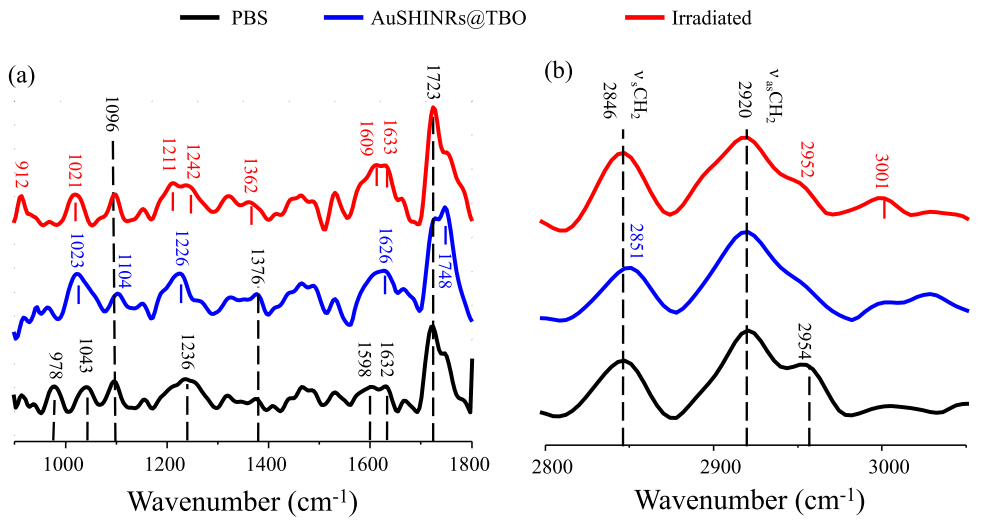

Figure 3. PM-IRRAS spectra recorded for neat Caco-2 lipid extract and cospread AuSHINRs@TBO: Caco-2 (1:1 v/v) monolayers before and after irradiation. The measurements were carried out on the PBS subphase at 30 mN/m. The spectra were split to highlight the vibrational modes of the (a) polar heads and (b) aliphatic chains.

was observed between 0 and 30 mN/m, suggesting that extract heterogeneity does not adversely affect molecular accommodation, even under high packing conditions. At 0 mN/m, films containing AuSHINRs@TBO showed no discernible morphological difference, suggesting they do not induce self-aggregation or organizational changes in lipid structures. However, as the pressure increased up to 30 mN/m and the films became more tightly packed, significant domains emerged, indicating that AuSHINRs@TBO alter the initial organization of lipid molecules. These molecular-level interactions were investigated via PM-IRRAS, as discussed later on.

Figure 3 displays the PM-IRRAS spectra recorded for neat Caco-2 lipid extract and the cospread AuSHINRs@TBO: Caco-2 (1:1 v/v) monolayers. The assignments of the main vibrational modes and the shifts caused by AuSHINRs@TBO are listed in Table 3. The hydrophilic groups show more pronounced alterations in Figure 3a owing to a larger nanorod insertion compared with the aliphatic chains. For instance, there were significant effects on the phosphate groups, with $\upsilon_{as}(C-O-PO_2^-)$ at 1043 cm^{-1}, $\upsilon_s(PO_2^-)$ at 1096 cm^{-1}, and $\upsilon_{as}(PO_2^-)$ at 1236 cm^{-1} shifting to 1023, 1104, and 1226 cm^{-1}, respectively. Comparable shifts were reported for synthetic monolayers on AuSHINRs colloidal suspension[53] and TBO subphase,[60] ascribed to the electrostatic nature of adsorption. The shift of $\upsilon_{as}(PO_2^-)$ to lower wavenumbers implies hydration of the phosphate groups in the films.[65] Additionally, modifications in the $\upsilon_{as}(C-O-PO_2^-)$ group were accompanied by a large increase in the band intensity in the presence of AuSHINRs@TBO, indicating changes in the molecular organization. A similar effect was observed for the $\upsilon_{as}(CN^+(CH_3)_3)$ band at 978 cm^{-1}, which was no longer discernible in the Caco-2 film containing AuSHINRs@TBO. The region between 1600 and 1700 cm^{-1} characterizes water interface reflectivity.[66,67] The carbonyl ester band initially appears as a doublet at 1723 and 1748 cm^{-1}, representing hydrated and nonhydrated stretching, respectively. Upon the incorporation of AuSHINRs@TBO, there is an increase in relative intensity at 1748 cm^{-1}, indicating dehydration of the monolayer.

Table 3. Assignments of the Principal Vibrational Modes of Neat Caco-2 Lipid Extract Monolayers and Shifts Induced upon AuSHINRs@TBO (1:1 v/v) Incorporation and Irradiation

assignments	Caco-2 lipid extract monolayers		
	neat	+ AuSHINRs@TBO	
		nonirradiated	irradiated
$\delta\ (NH_3^+)_{rocking} + \upsilon(CN)$			912
$\upsilon_{as}\ CN^+(CH_3)_3$	978		
$\upsilon_{as}\ (C-O-PO_2^-)$	1043	1023	1021
$\upsilon_s\ (PO_2^-)$	1096	1104	1098
$\upsilon_{as}\ (PO_2^-)$	1236	1226	1242
$\delta_s\ (CH_3)$	1376	1376	1362
$\delta(H_2O)$	1598	1626	1609
	1632		1633
$\upsilon\ (C-O)$	1723	1728	1726
	1748	1748	1752
$\upsilon_s\ (CH_2)$	2846	2851	2846
$\upsilon_{as}\ (CH_2)$	2920	2920	2920
$\upsilon_{as}\ (CH_3)$	2954		2952
$\upsilon\ (HC{=}CH)$			3001

The incorporation of AuSHINRs@TBO induced minimal changes in the aliphatic chain, as shown in Figure 3b. A slight modification was observed in the $\upsilon_s(CH_2)$ band, shifting from 2846 to 2851 cm^{-1}. The $\upsilon_s(CH_2)$ and $\upsilon_{as}(CH_2)$ intensity ratio (I_s/I_{as}) increased from 0.66 to 0.84, indicating a decrease in the order of hydrocarbon chains, while the $\upsilon_{as}(CH_3)$ band at 2954 cm^{-1} was no longer observed. Therefore, the insertion of AuSHINRs@TBO is primarily governed by electrostatic interactions with the polar region of the Caco-2 monolayer, as repulsive forces from cationic groups, such as choline, prevent deeper penetration. The attractive forces with phosphate groups leading to adsorption onto the monolayer induce dehydration of carbonyl groups and alterations in aliphatic chain ordering, as indicated in Figure 4b.

Photoinduced Effects of AuSHINRs@TBO on Caco-2 Lipid Extract Monolayers. The impact of AuSHINRs@TBO (1:1 v/v) on Caco-2 lipid extract monolayers under light irradiation was assessed by measuring the relative surface area

https://doi.org/10.1021/acsami.4c02247
ACS Appl. Mater. Interfaces XXXX, XXX, XXX−XXX

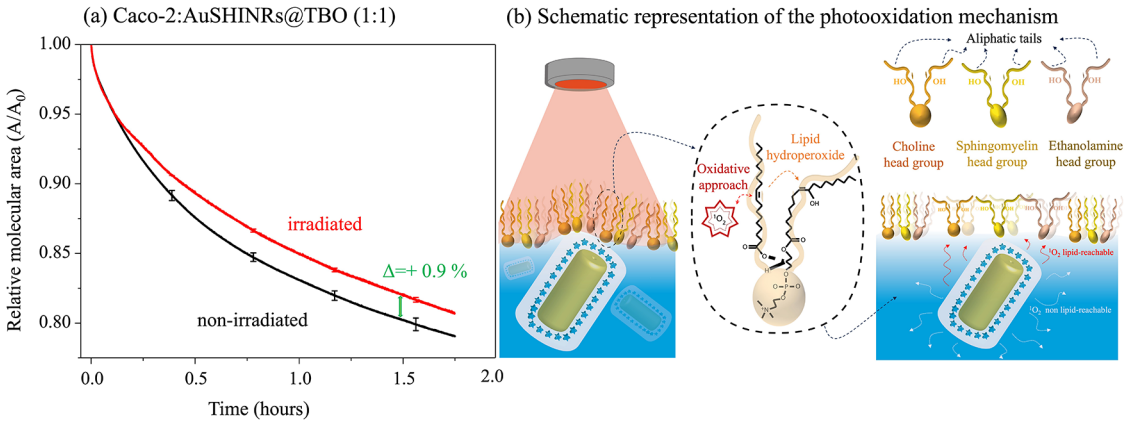

Figure 4. (a) Relative area (A/A_0) progression of irradiated and nonirradiated Caco-2: AuSHINRs@TBO (1:1 v/v) monolayers recorded at 30 mN/m. (b) Schematic representation of the photooxidation mechanism of AuSHINRs@TBO in Caco-2 lipid extract monolayers.

progression (A/A_0) at a constant pressure of 30 mN/m, as depicted in Figure 4a. While irradiation alone did not cause a significant effect on neat Caco-2 monolayers, an area decrease was observed for nonirradiated monolayers owing to the material loss attributed to the uncontrolled oxidation with reactive oxygen species (ROS) in the environment.[68] The rate of material loss decreased upon irradiation, indicating an increased stability of the monolayers. The difference between the irradiated and nonirradiated (Δ) curves suggested a general increase in the area occupied by the extract by ca. 1.0%. AuSHINRs sustain localized surface plasmon resonance (LSPR) upon near-infrared light excitation, leading to a localized temperature increase resulting from the collective oscillations of electrons.[5] In a previous work, we showed that irradiated AuSHINRs generate excited electrons that subsequently decay into hot electrons, sensitizing molecular oxygens (O_2) and initiating the production of ROS by either energy or electron transfer.[53] Furthermore, TBO initiates type II reactions, producing singlet oxygen ($^1O_2$) capable of creating hydroperoxide groups in the vicinity of phospholipid unsaturation.[60,69,70] Therefore, the synergistic effect of AuSHINRs and TBO upon irradiation is expected to enhance ROS generation including $^1O_2$. This can lead to hydroperoxidation reactions, aligning with the observed increase in surface area of the irradiated monolayers containing AuSHINRs@TBO. Such area increase, while not highly significant, is likely attributed to the inherent complexity of the cell extract. Similar challenges have been documented in recent studies involving tumor lipid extract monolayers, where obtaining more pronounced effects proved intricate.[71,72] An illustrative model of the binding mechanism and impact of the photoreaction is presented in Figure 4b.

Irradiation of Caco-2 lipid extract monolayers containing AuSHINRs@TBO (1:1 v/v) causes significant changes in the PM-IRRAS, especially in the head groups, as shown in Figure 3. For example, the $\upsilon_{as}(C-O-PO_2^-)$ band persisted at 1021 cm^{-1}, while $\upsilon_s(PO_2^-)$ returned to its original vibration at 1098 cm^{-1}. A distinct vibrational group emerged at 912 cm^{-1}, corresponding to the NH_3^+ rocking and C−N stretching mode, characteristic of phosphatidylserines.[47] The CH_3 bending shifted from 1376 to 1362 cm^{-1}. The phosphate group previously at 1226 cm^{-1} split into two bands at 1211 and 1242 cm^{-1}, related to the hydration and dehydration of these groups, respectively. Furthermore, the vibrational mode associated with hydrated carbonyl becomes more pronounced at 1726 cm^{-1}. In the aliphatic groups, changes in the vibrational maximum are limited to the reappearance of the CH_3 band at 2952 cm^{-1}. The $\upsilon_s(CH_2)$ and $\upsilon_{as}(CH_2)$ intensity ratio (I_s/I_{as}) decreased from 0.84 to 0.57, indicating an increased order of the carbon chains. The changes in the PM-IRRAS spectra induced by irradiation suggest modifications in packing of the monolayer, although the precise details of such modifications cannot be determined with the present results. They are nevertheless consistent with formation of hydroperoxide groups which occur when unsaturated chains are attacked by $^1O_2$. A scheme representing the impact of the oxidative reactions on the monolayer organization is depicted in Figure 4b.

Photoinduced Impact on Caco-2 Cell Cultures by AuSHINRs@TBO. Mitochondrial metabolic activity tests (MTT) were performed on Caco-2 cell cultures following exposure to irradiated and nonirradiated AuSHINRs and AuSHINRs@TBO. The colloids were diluted in culture medium at different volumetric ratios (1:10, 1:9, 1:8, and 1:7 v/v) to mitigate the inherent toxicity attributed to the CTAB surfactant utilized in AuNR synthesis.[73] Figure 5a shows a slight reduction in cell viability in the absence of light for AuSHINRs, contrasting with the significant decrease observed for AuSHINRs@TBO in Figure 5b at 1:8 and 1:7 dilution ratios. Caco-2 cultures containing AuSHINRs displayed minimal susceptibility to phototoxic effects, with the most notable reduction in viability observed at the 1:7 dilution ratio, from 90.2 to 77.7%. To overcome the inherent toxicity of gold nanorods and improve photothermal efficiency, Huang et al. increased specificity of the nanostructures by introducing specific antibodies onto their surface.[74] Indeed, achieving a substantial impact on tumor cell cultures through photothermal effects requires heat induction exceeding 43 °C owing to the elevated survival rates below this temperature.[75] At such a dilution ratio (1:7 v/v) of AuSHINRs, it is possible that not only the photothermal efficiency but also the generation of ROS might have been significantly diminished. On the other hand, the incorporation of AuSHINRs@TBO increased the phototoxic effect, noticeable even at the most diluted ratio (1:10 v/v), leading to a viability decrease from 87.5 to 39.0%. These observations revealed a synergistic effect, wherein AuSHINRs@TBO enhanced ROS generation with a combination of photothermal effects and oxidative reactions. Jang et al.[76] explored a similar gold nanorod and photosensitizer (AlPcS4) conjugation approach. They found that these

https://doi.org/10.1021/acsami.4c02247
ACS Appl. Mater. Interfaces XXXX, XXX, XXX−XXX

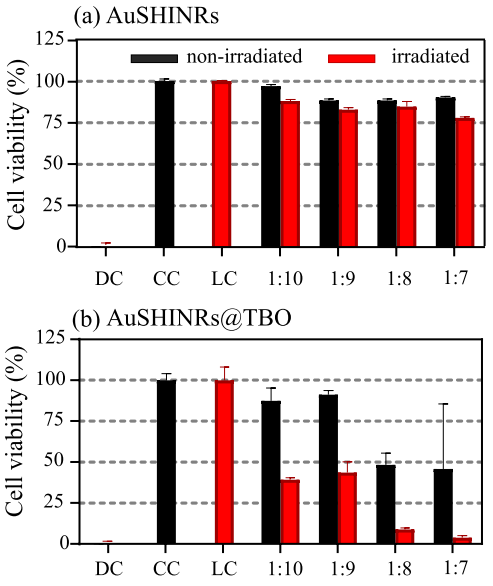

Figure 5. Caco-2 cell viability upon irradiated and nonirradiated (a) AuSHINRs and (b) AuSHINRs@TBO at 1:10, 1:9, 1:8, and 1:7 volumetric dilution ratios (v/v in culture medium).

nanoparticles efficiently delivered AlPcS4 to target cells, enhancing their inhibitory effect on squamous cell carcinoma (SCC7). However, their study did not evaluate photothermal effects, and the conjugated nanoparticles lacked fluorescence, suggesting quenching.

Morphological changes induced by the interaction and irradiation of Caco-2 cells cultured with AuSHINRs and AuSHINRs@TBO were assessed via confocal fluorescence microscopy. The investigation centered on dilution ratios 1:9 and 1:8 v/v in the culture medium, with the identified changes highlighted through the nucleus (blue) and plasma membrane (green) staining. Relative to the control group, AuSHINRs caused minor morphological modifications in both dilutions (1:9 and 1:8 v/v), as evidenced by uniform nuclei and well-defined plasma membranes in the microscopies. Minor changes in membrane labeling were evident following incubation with AuSHINRs@TBO at a 1:8 dilution ratio, possibly indicative of the observed cytotoxicity in the MTT assays. The influence of nanostructure photoactivation on Caco-2 cells was evaluated after a 1 h irradiation. As shown in Figure 6, irradiation alone had minimal effects on the integrity of the cell nucleus and membrane, similar to the observed for the irradiated groups containing AuSHINRs. This consistency in minimal impact is indicative of the low phototoxic effects of AuSHINRs and can be attributed to the dilution effect, as there is a correlation between nanostructure concentration and heat generation.[33] In contrast, irradiated AuSHINRs@TBO induced significant modifications associated with nanostructure phototoxicity owing to the synergistic effect. At a ratio of 1:9 v/v, membranes displayed heightened fibrous characteristics, while at a ratio of 1:8 v/v, both the cell membrane and nuclei exhibited fragmentation. The observed fibrous characteristics align with the AuSHINRs@TBO adsorption observed on the Langmuir monolayer, suggesting that the plasma membrane is a primary target for therapeutic intervention. The fragmentation of both the plasma membrane and the nuclei suggests that cells containing irradiated AuSHINRs@TBO undergo necrosis. Indeed, the necrotic pathway, which involves cellular swelling, loss of plasma membrane integrity with organelle edema, and nuclear alterations (pyknosis) or absence, is a well-documented mechanism induced by hyperthermia.[77]

CONCLUSIONS

Langmuir films were employed here to construct biomembranes using cell lipid extract from Caco-2, aiming to assess the mechanisms underlying the photoefficiency of gold shell-isolated nanorods conjugated with toluidine blue-O (AuSHINRs@TBO). The observed isotherm expansion upon AuSHINRs@TBO interaction, along with PM-IRRAS data, suggested an electrostatic attraction between the positively charged nanostructures and the negatively charged domains of the lipid groups, influencing not only the polar lipid heads but also the ordering of the aliphatic chains. Brewster angle microscopy revealed that the 1:1 v/v Caco-2: AuSHINRs@TBO films induced notable morphological changes, suggesting particle-driven reorganization within the monolayer at a

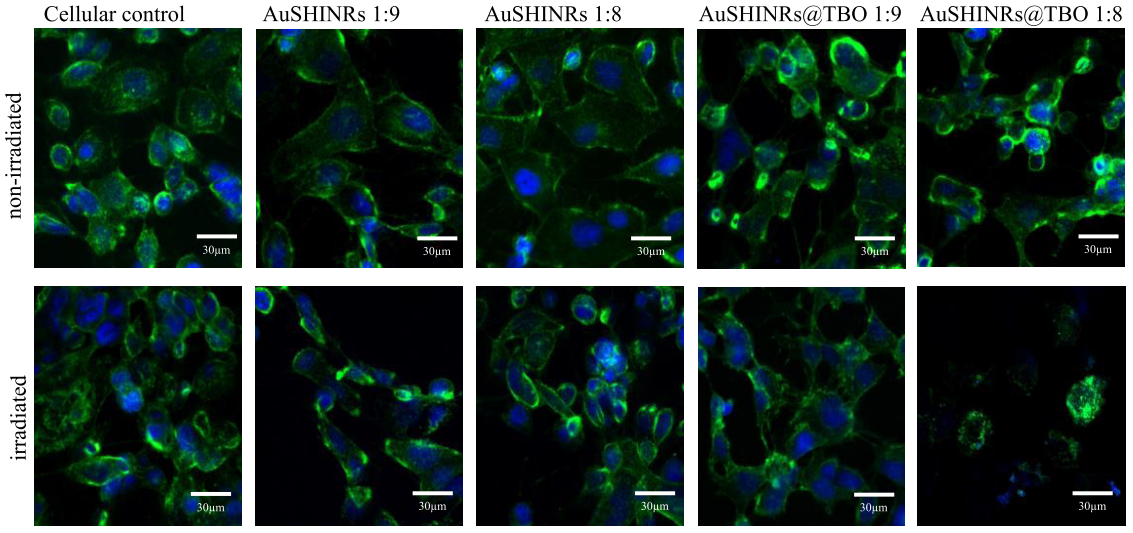

Figure 6. Confocal microscopies of Caco-2 cellular control and 24 h incubation with irradiated and nonirradiated AuSHINRs and AuSHINRs@TBO at 1:9 and 1:8 v/v dilution ratios. Irradiation was at 640 nm with an irradiance of 20 mW/cm^2. The nucleus was labeled using DAPI (in blue), and the membrane was stained with WGA (in green).

https://doi.org/10.1021/acsami.4c02247
ACS Appl. Mater. Interfaces XXXX, XXX, XXX−XXX

surface pressure of 30 mN/m. Light irradiation decreased the rate of material loss of Caco-2 monolayers containing AuSHINRs@TBO (1:1 v/v), suggesting enhanced stability and a more expansive area covered by the film. The combined action of AuSHINRs and TBO under irradiation is anticipated to boost ROS production, especially singlet oxygens ($^1O_2$). Hence, the monolayer expansion correlates with an increased spatial distribution of molecules owing to the hydroperoxide generation prompted by the $^1O_2$ attack to the chain unsaturation. *In vitro* experiments identified inherent cytotoxicity from the CTAB surfactant in the nanostructures, necessitating serial dilutions to alleviate these effects in Caco-2 cultures. TBO-conjugated nanoparticles demonstrated a marked increase in phototoxic effects, evident even at the most diluted ratio of 1:10 v/v, which resulted in a significant reduction in cell viability from 87.5 to 39.0%. This outcome underscores a synergistic effect where the TBO-conjugated nanorods amplified ROS production, effectively merging photothermal effects with oxidative reactions. Confocal fluorescence microscopy pinpointed the cell membranes as the primary site of action for inducing cell death, marked by morphological changes and increased fibrous features. In summary, this work sheds light on the complex interactions and effects within a bioinspired membrane system, highlighting the potential of TBO-conjugated nanorods in advancing cancer therapy through synergistic PTT and PDT.

■ ASSOCIATED CONTENT

Supporting Information

The Supporting Information is available free of charge at https://pubs.acs.org/doi/10.1021/acsami.4c02247.

Additional histograms of average nanoparticle dimensions and table of hydrodynamic diameter measurements of AuSHINRs@TBO (PDF)

■ AUTHOR INFORMATION

Corresponding Author

Alexandre Mendes de Almeida Junior − *School of Sciences, Humanities and Languages, São Paulo State University (UNESP), Assis, SP 19806-900, Brazil;* orcid.org/0000-0002-7063-0812; Email: alexjunior.biotec@gmail.com

Authors

André Satoshi Ferreira − *School of Sciences, Humanities and Languages, São Paulo State University (UNESP), Assis, SP 19806-900, Brazil*

Sabrina Aléssio Camacho − *School of Sciences, Humanities and Languages, São Paulo State University (UNESP), Assis, SP 19806-900, Brazil; São Carlos Institute of Physics, University of São Paulo (USP), São Carlos, SP 13566-590, Brazil*

Lucas Gontijo Moreira − *School of Sciences, Humanities and Languages, São Paulo State University (UNESP), Assis, SP 19806-900, Brazil*

Karina Alves de Toledo − *School of Sciences, Humanities and Languages, São Paulo State University (UNESP), Assis, SP 19806-900, Brazil*

Osvaldo N. Oliveira, Jr. − *São Carlos Institute of Physics, University of São Paulo (USP), São Carlos, SP 13566-590, Brazil;* orcid.org/0000-0002-5399-5860

Pedro Henrique Benites Aoki − *School of Sciences, Humanities and Languages, São Paulo State University (UNESP), Assis, SP 19806-900, Brazil;* orcid.org/0000-0003-4701-6408

Complete contact information is available at: https://pubs.acs.org/10.1021/acsami.4c02247

Notes

The authors declare no competing financial interest.

■ ACKNOWLEDGMENTS

This work was supported by CNPq and FAPESP (2018/22214-6, 2021/14500-1, 2022/02189-2). A.M.A. Jr. is thankful for his scholarship provided by CAPES and A.S.F. (2023/01999-3), S.A.C. (2018/14692-5), and L.G.M. (2020/15854-9) are thankful for their scholarship provided by FAPESP. We thank Dr. Carlos J. L. Constantino for the assistance with the confocal imaging (EMU 2014/11408-3).

■ REFERENCES

(1) Gu, X.; Timchenko, V.; Yeoh, G. H.; Dombrovsky, L.; Taylor, R. The Effect of Gold Nanorods Clustering on Near-Infrared Radiation Absorption. *Appl. Sci.* **2018**, *8* (7), 1132 DOI: 10.3390/app8071132.

(2) Cai, Z.; Zhang, Y.; He, Z.; Jiang, L. P.; Zhu, J. J. NIR-Triggered Chemo-Photothermal Therapy by Thermosensitive Gold Nanostar@Mesoporous Silica@Liposome-Composited Drug Delivery Systems. *ACS Appl. Bio Mater.* **2020**, *3* (8), 5322−5330.

(3) Lv, Z.; He, S.; Wang, Y.; Zhu, X. Noble Metal Nanomaterials for NIR-Triggered Photothermal Therapy in Cancer. *Adv. Healthcare Mater.* **2021**, 2001806 DOI: 10.1002/adhm.202001806.

(4) Huang, X.; Jain, P. K.; El-Sayed, I. H.; El-Sayed, M. A. Plasmonic Photothermal Therapy (PPTT) Using Gold Nanoparticles. *Lasers Med. Sci.* **2008**, *23*, 217−228.

(5) Petryayeva, E.; Krull, U. J. Localized Surface Plasmon Resonance: Nanostructures, Bioassays and Biosensing-A Review. *Anal. Chim. Acta* **2011**, *706*, 8−24.

(6) Svaasand, L. O.; Gomer, C. J.; Morinelli, E. On the Physical Rationale of Laser Induced Hyperthermia. *Laser Med. Sci.* **1990**, *5*, 121−128.

(7) Xia, B.; Wang, B.; Shi, J.; Zhang, Y.; Zhang, Q.; Chen, Z.; Li, J. Photothermal and Biodegradable Polyaniline/Porous Silicon Hybrid Nanocomposites as Drug Carriers for Combined Chemo-Photothermal Therapy of Cancer. *Acta Biomater.* **2017**, *51*, 197−208.

(8) Ali, A. A.; Abuwatfa, W. H.; Al-Sayah, M. H.; Husseini, G. A. Gold-Nanoparticle Hybrid Nanostructures for Multimodal Cancer Therapy. *Nanomaterials* **2022**, *12* (20), 3706.

(9) Costantini, P. E.; Di Giosia, M.; Ulfo, L.; Petrosino, A.; Saporetti, R.; Fimognari, C.; Pompa, P. P.; Danielli, A.; Turrini, E.; Boselli, L.; Calvaresi, M. Spiky Gold Nanoparticles for the Photothermal Eradication of Colon Cancer Cells. *Nanomaterials* **2021**, *11* (6), 1608.

(10) Nejati, K.; Dadashpour, M.; Gharibi, T.; Mellatyar, H.; Akbarzadeh, A. Biomedical Applications of Functionalized Gold Nanoparticles: A Review. *J. Cluster Sci.* **2022**, *33*, 1−16, DOI: 10.1007/s10876-020-01955-9.

(11) Wang, J.; Zhu, C.; Han, J.; Han, N.; Xi, J.; Fan, L.; Guo, R. Controllable Synthesis of Gold Nanorod/Conducting Polymer Core/Shell Hybrids Toward in Vitro and in Vivo near-Infrared Photothermal Therapy. *ACS Appl. Mater. Interfaces* **2018**, *10* (15), 12323−12330.

(12) Wang, J.; Han, J.; Zhu, C.; Han, N.; Xi, J.; Fan, L.; Guo, R. Gold Nanorods/Polypyrrole/m-SiO 2 Core/Shell Hybrids as Drug Nanocarriers for Efficient Chemo-Photothermal Therapy. *Langmuir* **2018**, *34* (48), 14661−14669.

(13) Ahmed, K.; Zaidi, S. F.; Mati-ur-Rehman; Rehman, R.; Kondo, T. Hyperthermia and Protein Homeostasis: Cytoprotection and Cell Death. *J. Therm. Biol.* **2020**, *33*, 1−16, DOI: 10.1016/j.jtherbio.2020.102615.

(14) Hildebrandt, B.; Wust, P.; Ahlers, O.; Dieing, A.; Sreenivasa, G.; Kerner, T.; Felix, R.; Riess, H. The Cellular and Molecular Basis of

Hyperthermia. *Critical Rev. Oncol./Hematol.* **2002**, *43*, 33−56, DOI: 10.1016/s1040-8428(01)00179-2.
(15) Lepock, J. R. Cellular Effects of Hyperthermia: Relevance to the Minimum Dose for Thermal Damage. *Int. J. Hyperthermia* **2003**, *19* (3), 252−266.
(16) Bartneck, M.; Keul, H. A.; Singh, S.; Czaja, K.; Bornemann, J.; Bockstaller, M.; Moeller, M.; Zwadlo-Klarwasser, G.; Groll, J. Rapid Uptake of Gold Nanorods by Primary Human Blood Phagocytes and Immunomodulatory Effects of Surface Chemistry. *ACS Nano* **2010**, *4* (6), 3073−3086.
(17) Liu, X.; Huang, N.; Li, H.; Wang, H.; Jin, Q.; Ji, J. Multidentate Polyethylene Glycol Modified Gold Nanorods for in Vivo Near-Infrared Photothermal Cancer Therapy. *ACS Appl. Mater. Interfaces* **2014**, *6* (8), 5657−5668.
(18) Barreto, Â.; Luis, L. G.; Girão, A. V.; Trindade, T.; Soares, A. M. V. M.; Oliveira, M. Behavior of Colloidal Gold Nanoparticles in Different Ionic Strength Media. *J. Nanopart. Res.* **2015**, *17* (12), 1−13.
(19) Liu, J.; Kan, C.; Cong, B.; Xu, H.; Ni, Y.; Li, Y.; Shi, D. Plasmonic Property and Stability of Core-Shell Au@SiO2 Nanostructures. *Plasmonics* **2014**, *9* (5), 1007−1014.
(20) Hanske, C.; Sanz-Ortiz, M. N.; Liz-Marzán, L. M. Silica-Coated Plasmonic Metal Nanoparticles in Action. *Adv. Mater.* **2018**, *30*, 1707003 DOI: 10.1002/adma.201707003.
(21) Liu, J.; Kan, C.; Cong, B.; Xu, H.; Ni, Y.; Li, Y.; Shi, D. Plasmonic Property and Stability of Core-Shell Au@SiO2 Nanostructures. *Plasmonics* **2014**, *9* (5), 1007−1014.
(22) Kharkwal, G. B.; Sharma, S. K.; Huang, Y. Y.; Dai, T.; Hamblin, M. R. Photodynamic Therapy for Infections: Clinical Applications. *Lasers Surg. Med.* **2011**, *43*, 755−767.
(23) Dąbrowski, J. M.; Arnaut, L. G. Photodynamic Therapy (PDT) of Cancer: From Local to Systemic Treatment. *Photochem. Photobiol. Sci.* **2015**, *14*, 1765−1780, DOI: 10.1039/c5pp00132c.
(24) Zou, Z.; Chang, H.; Li, H.; Wang, S. Induction of Reactive Oxygen Species: An Emerging Approach for Cancer Therapy. *Apoptosis* **2017**, *22*, 1321−1335, DOI: 10.1007/s10495-017-1424-9.
(25) Demidova, T. N.; Hamblin, M. R. Photodynamic Therapy Targeted to Pathogens. *Int. J. Immunopathol. Pharmacol.* **2004**, *17* (3), 245−254.
(26) Redrado, M.; Benedi, A.; Marzo, I.; Gimeno, M. C.; Fernández-Moreira, V. Dual Emissive Ir(Iii) Complexes for Photodynamic Therapy and Bioimaging. *Pharmaceutics* **2021**, *13* (9), 1382.
(27) Arnaut, L. G.; Pereira, M. M.; Dąbrowski, J. M.; Silva, E. F. F.; Schaberle, F. A.; Abreu, A. R.; Rocha, L. B.; Barsan, M. M.; Urbańska, K.; Stochel, G.; Brett, C. M. A. Photodynamic Therapy Efficacy Enhanced by Dynamics: The Role of Charge Transfer and Photostability in the Selection of Photosensitizers. *Chem.—Eur. J.* **2014**, *20* (18), 5346−5357.
(28) Abels, C. Targeting of the Vascular System of Solid Tumours by Photodynamic Therapy (PDT). *Photochem. Photobiol. Sci.* **2004**, *3* (8), 765−771.
(29) Agostinis, P.; Berg, K.; Cengel, K. A.; Foster, T. H.; Girotti, A. W.; Gollnick, S. O.; Hahn, S. M.; Hamblin, M. R.; Juzeniene, A.; Kessel, D.; Korbelik, M.; Moan, J.; Mroz, P.; Nowis, D.; Piette, J.; Wilson, B. C.; Golab, J. Photodynamic Therapy of Cancer: An Update. *CA Cancer J. Clin.* **2011**, *61* (4), 250−281.
(30) Dougherty, T. J.; Gomer, C. J.; Henderson, B. W.; Jori, G.; Kessel, D.; Korbelik, M.; Moan, J.; Peng, Q. Photodynamic Therapy. *J. Natl. Cancer Inst.* **1998**, *90* (12), 889−905.
(31) Cárdenas, G.; Nogueira, J. J. Stacking Effects on Anthraquinone/DNA Charge-Transfer Electronically Excited States. *Molecules* **2020**, *25* (24), 5927.
(32) Montaseri, H.; Kruger, C. A.; Abrahamse, H. Inorganic Nanoparticles Applied for Active Targeted Photodynamic Therapy of Breast Cancer. *Pharmaceutics.* **2021**, *13* (3), 296 DOI: 10.3390/pharmaceutics13030296.
(33) Sun, M.; Peng, D.; Hao, H.; Hu, J.; Wang, D.; Wang, K.; Liu, J.; Guo, X.; Wei, Y.; Gao, W. Thermally Triggered in Situ Assembly of Gold Nanoparticles for Cancer Multimodal Imaging and Photothermal Therapy. *ACS Appl. Mater. Interfaces* **2017**, *9* (12), 10453−10460.
(34) Abrahamse, H.; Hamblin, M. R. New Photosensitizers for Photodynamic Therapy. *Biochem. J.* **2016**, *473*, 347−364, DOI: 10.1042/BJ20150942.
(35) Gai, S.; Yang, G.; Yang, P.; He, F.; Lin, J.; Jin, D.; Xing, B. Recent Advances in Functional Nanomaterials for Light−Triggered Cancer Therapy. *Nano Today* **2018**, *19*, 146−187, DOI: 10.1016/j.nantod.2018.02.010.
(36) Ilanchelian, M.; Ramaraj, R. Binding Interactions of Toluidine Blue O with *Escherichia Coli* DNA: Formation of Bridged Structure. *J. Fluoresc* **2011**, *21* (4), 1439−1453.
(37) Usacheva, M. N.; Teichert, M. C.; Sievert, C. E.; Biel, M. A. Effect of Ca2+ on the Photobactericidal Efficacy of Methylene Blue and Toluidine Blue against Gram-Negative Bacteria and the Dye Affinity for Lipopolysaccharides. *Lasers Surg Med.* **2006**, *38* (10), 946−954.
(38) Sung, H.; Ferlay, J.; Siegel, R. L.; Laversanne, M.; Soerjomataram, I.; Jemal, A.; Bray, F. Global Cancer Statistics 2020: GLOBOCAN Estimates of Incidence and Mortality Worldwide for 36 Cancers in 185 Countries. *CA Cancer J. Clin.* **2021**, *71* (3), 209−249.
(39) Monteiro-Cardoso, V. F.; Silva, A. M.; Oliveira, M. M.; Peixoto, F.; Videira, R. A. Membrane Lipid Profile Alterations Are Associated with the Metabolic Adaptation of the Caco-2 Cells to Aglycemic Nutritional Condition. *J. Bioenerg. Biomembr.* **2014**, *46* (1), 45−57.
(40) Menendez, J. A.; Lupu, R. Fatty Acid Synthase and the Lipogenic Phenotype in Cancer Pathogenesis. *Nat. Rev. Cancer* **2007**, *7*, 763−777.
(41) Aroca, R. F.; Teo, G. Y.; Mohan, H.; Guerrero, A. R.; Albella, P.; Moreno, F. Plasmon-Enhanced Fluorescence and Spectral Modification in SHINEF. *J. Phys. Chem. C* **2011**, *115* (42), 20419−20424.
(42) Grandi, S.; Tomasi, C.; Mustarelli, P.; Clemente, F.; Carbonaro, C. M. Characterisation of a New Sol-Gel Precursor for a SiO2-Rhodamine 6G Hybrid Class II Material. *J. Solgel Sci. Technol.* **2007**, *41* (1), 57−63.
(43) Oliveira, O. N.; Caseli, L.; Ariga, K. The Past and the Future of Langmuir and Langmuir-Blodgett Films. *Chem. Rev.* **2022**, *122*, 6459−6513, DOI: 10.1021/acs.chemrev.1c00754.
(44) Nikoobakht, B.; El-Sayed, M. A. Preparation and Growth Mechanism of Gold Nanorods (NRs) Using Seed-Mediated Growth Method. *Chem. Mater.* **2003**, *15* (10), 1957−1962.
(45) Huang, X.; El-Sayed, M. A. Gold Nanoparticles: Optical Properties and Implementations in Cancer Diagnosis and Photothermal Therapy. *J. Adv. Res.* **2010**, *1* (1), 13−28.
(46) Sun, Q.; Shi, X.; Feng, J.; Zhang, Q.; Ao, Z.; Ji, Y.; Wu, X.; Liu, D.; Han, D. Cytotoxicity and Cellular Responses of Gold Nanorods to Smooth Muscle Cells Dependent on Surface Chemistry Coupled Action. *Small* **2018**, *14* (52), 1803715 DOI: 10.1002/smll.201803715.
(47) Camacho, S. A.; Kobal, M. B.; Almeida, A. M.; Toledo, K. A.; Oliveira, O. N.; Aoki, P. H. B. Molecular-Level Effects on Cell Membrane Models to Explain the Phototoxicity of Gold Shell-Isolated Nanoparticles to Cancer Cells. *Colloids Surf. B Biointerfaces* **2020**, *194*, 111189.
(48) Cai, W.; Gao, T.; Hong, H.; Sun, J. Applications of Gold Nanoparticles in Cancer Nanotechnology. *Nanotechnol Sci. Appl.* **2008**, *Volume 1*, 17−32.
(49) An, J.; Yang, X. Q.; Cheng, K.; Song, X. L.; Zhang, L.; Li, C.; Zhang, X. S.; Xuan, Y.; Song, Y. Y.; Fang, B. Y.; Hou, X. L.; Zhao, Y. Di.; Liu, B. In Vivo Computed Tomography/Photoacoustic Imaging and NIR-Triggered Chemo-Photothermal Combined Therapy Based on a Gold Nanostar-, Mesoporous Silica-, and Thermosensitive Liposome-Composited Nanoprobe. *ACS Appl. Mater. Interfaces* **2017**, *9* (48), 41748−41759.
(50) Monem, A. S.; Elbialy, N.; Mohamed, N. Mesoporous Silica Coated Gold Nanorods Loaded Doxorubicin for Combined Chemo-Photothermal Therapy. *Int. J. Pharm.* **2014**, *470* (1−2), 1−7.

https://doi.org/10.1021/acsami.4c02247
ACS Appl. Mater. Interfaces XXXX, XXX, XXX−XXX

(51) Zhang, Z.; Wang, L.; Wang, J.; Jiang, X.; Li, X.; Hu, Z.; Ji, Y.; Wu, X.; Chen, C. Mesoporous Silica-Coated Gold Nanorods as a Light-Mediated Multifunctional Theranostic Platform for Cancer Treatment. *Adv. Mater.* **2012**, *24* (11), 1418−1423.
(52) Gao, Z.; Burrows, N. D.; Valley, N. A.; Schatz, G. C.; Murphy, C. J.; Haynes, C. L. In Solution SERS Sensing Using Mesoporous Silica-Coated Gold Nanorods. *Analyst* **2016**, *141* (17), 5088−5095.
(53) Almeida, A. M., Jr.; Moreira, L. G.; Camacho, S. A.; Ferreira, F. G.; Conceição, K.; Tada, D. B.; Aoki, P. H. B. Photochemical Outcomes Triggered by Gold Shell-Isolated Nanorods on Bioinspired Nanoarchitectonics for Bacterial Membranes. *Biochim. Biophys. Acta, Biomembr.* **2023**, *1865* (8), 184216.
(54) Fort, E.; Grésillon, S. Surface Enhanced Fluorescence. *J. Phys. D Appl. Phys.* **2008**, *41* (1), 013001.
(55) Ayala-Orozco, C.; Liu, J. G.; Knight, M. W.; Wang, Y.; Day, J. K.; Nordlander, P.; Halas, N. J. Fluorescence Enhancement of Molecules inside a Gold Nanomatryoshka. *Nano Lett.* **2014**, *14* (5), 2926−2933.
(56) Camacho, S. A.; Sobral-Filho, R. G.; Aoki, P. H. B.; Constantino, C. J. L.; Brolo, A. G. Immunoassay Quantification Using Surface-Enhanced Fluorescence (SEF) Tags. *Analyst* **2017**, *142* (15), 2717−2724.
(57) Gersten, J.; Nitzan, A. Spectroscopic Properties of Molecules Interacting with Small Dielectric Particles. *J. Chem. Phys.* **1981**, *75* (3), 1139−1152.
(58) Lakowicz, J. R. Radiative Decay Engineering: Biophysical and Biomedical Applications. *Anal. Biochem.* **2001**, *298* (1), 1−24.
(59) Zhang, Z.; Maji, S.; Antunes, A. B. D. F.; De Rycke, R.; Zhang, Q.; Hoogenboom, R.; De Geest, B. G. Salt Plays a Pivotal Role in the Temperature-Responsive Aggregation and Layer-by-Layer Assembly of Polymer-Decorated Gold Nanoparticles. *Chem. Mater.* **2013**, *25* (21), 4297−4303.
(60) Almeida, A. M.; Oliveira, O. N.; Aoki, P. H. B. Role of Toluidine Blue-O Binding Mechanism for Photooxidation in Bioinspired Bacterial Membranes. *Langmuir* **2019**, *35* (51), 16745−16751.
(61) Szlasa, W.; Zendran, I.; Zalesińska, A.; Tarek, M.; Kulbacka, J. Lipid Composition of the Cancer Cell Membrane. *J. Bioenerg. Biomembr.* **2020**, *52*, 321−342.
(62) Ali, O.; Szabó, A. Review of Eukaryote Cellular Membrane Lipid Composition, with Special Attention to the Fatty Acids. *Int. J. Mol. Sci.* **2023**, *24*, 15693 DOI: 10.3390/ijms242115693.
(63) Doktorova, M.; Symons, J. L.; Levental, I. Structural and Functional Consequences of Reversible Lipid Asymmetry in Living Membranes. *Nat. Chem. Biol.* **2020**, 1321−1330, DOI: 10.1038/s41589-020-00688-0.
(64) Connor, J.; Bucana, C.; Fidler, I. J.; Schroit, A. J. Differentiation-Dependent Expression of Phosphatidylserine in Mammalian Plasma Membranes: Quantitative Assessment of Outer-Leaflet Lipid by Prothrombinase Complex Formation. *Proc. Natl. Acad. Sci. U.S.A.* **1989**, *86*, 3184 DOI: 10.1073/pnas.86.9.3184.
(65) Zawisza, I.; Lachenwitzer, A.; Zamlynny, V.; Horswell, S. L.; Goddard, J. D.; Lipkowski, J. Electrochemical and Photon Polarization Modulation Infrared Reflection Absorption Spectroscopy Study of the Electric Field Driven Transformations of a Phospholipid Bilayer Supported at a Gold Electrode Surface. *Biophys. J.* **2003**, *85* (6), 4055−4075.
(66) Aoki, P. H. B.; Morato, L. F. C.; Pavinatto, F. J.; Nobre, T. M.; Constantino, C. J. L.; Oliveira, O. N. Molecular-Level Modifications Induced by Photo-Oxidation of Lipid Monolayers Interacting with Erythrosin. *Langmuir* **2016**, *32* (15), 3766−3773.
(67) Hussein, N.; Lopes, C. C.; Pernambuco Filho, P. C. A.; Carneiro, B. R.; Caseli, L. Surface Chemistry and Spectroscopy Studies on 1,4-Naphthoquinone in Cell Membrane Models Using Langmuir Monolayers. *J. Colloid Interface Sci.* **2013**, *402*, 300−306.
(68) Liljeblad, J. F. D.; Bulone, V.; Tyrode, E.; Rutland, M. W.; Johnson, C. M. Phospholipid Monolayers Probed by Vibrational Sum Frequency Spectroscopy: Instability of Unsaturated Phospholipids. *Biophys. J.* **2010**, *98* (10), L50−L52, DOI: 10.1016/j.bpj.2010.02.009.
(69) Allison, R. R.; Sibata, C. H. Oncologic Photodynamic Therapy Photosensitizers: A Clinical Review. *Photodiagn. Photodyn. Ther.* **2010**, *7*, 61−75.
(70) Aoki, P. H. B.; Schroder, A. P.; Constantino, C. J. L.; Marques, C. M. Bioadhesive Giant Vesicles for Monitoring Hydroperoxidation in Lipid Membranes. *Soft Matter* **2015**, *11* (30), 5995−5998.
(71) Bistaffa, M. J.; Camacho, S. A.; Melo, C. F. O. R.; Catharino, R. R.; Toledo, K. A.; Aoki, P. H. B. Plasma Membrane Permeabilization to Explain Erythrosine B Phototoxicity on in Vitro Breast Cancer Cell Models. *J. Photochem. Photobiol. B* **2021**, *223*, 112297.
(72) Camacho, S. A.; Kobal, M. B.; Moreira, L. G.; Bistaffa, M. J.; Roque, T. C.; Pazin, W. M.; Toledo, K. A.; Oliveira, O. N.; Aoki, P. H. B. The Efficiency of Photothermal Action of Gold Shell-Isolated Nanoparticles against Tumor Cells Depends on Membrane Interactions. *Colloids Surf., B* **2022**, *211*, 112301.
(73) Choi, W. Il.; Sahu, A.; Kim, Y. H.; Tae, G. Photothermal Cancer Therapy and Imaging Based on Gold Nanorods. *Ann. Biomed. Eng.* **2012**, *40* (2), 534−546.
(74) Huang, X.; El-Sayed, I. H.; Qian, W.; El-Sayed, M. A. Cancer Cell Imaging and Photothermal Therapy in the Near-Infrared Region by Using Gold Nanorods. *J. Am. Chem. Soc.* **2006**, *128* (6), 2115−2120.
(75) Nejabat, M.; Samie, A.; Ramezani, M.; Alibolandi, M.; Abnous, K.; Taghdisi, S. M. An Overview on Gold Nanorods as Versatile Nanoparticles in Cancer Therapy. *J. Controlled Release* **2023**, *354*, 221−242, DOI: 10.1016/j.jconrel.2023.01.009.
(76) Jang, B.; Park, J. Y.; Tung, C. H.; Kim, I. H.; Choi, Y. Gold Nanorod-Photosensitizer Complex for near-Infrared Fluorescence Imaging and Photodynamic/Photothermal Therapy in Vivo. *ACS Nano* **2011**, *5* (2), 1086−1094.
(77) Krysko, D. V.; Vanden Berghe, T.; D'Herde, K.; Vandenabeele, P. Apoptosis and Necrosis: Detection, Discrimination and Phagocytosis. *Methods* **2008**, *44* (3), 205−221.

https://doi.org/10.1021/acsami.4c02247
ACS Appl. Mater. Interfaces XXXX, XXX, XXX−XXX